Damping of the collective modes in liquid Fe

Shinya Hosokawa*
Center for Materials Research using Third-Generation Synchrotron Radiation Facilities, Hiroshima Institute of Technology, Hiroshima 731-5193, Japan

Masanori Inui
Graduate School of Integrated Arts and Sciences, Hiroshima University, Higashi-Hiroshima 739-8521, Japan

Kazuhiro Matsuda
Department of Materials Science and Engineering, Graduate School of Engineering, Kyoto University, Kyoto 606-8501, Japan

Daisuke Ishikawa and Alfred Q. R. Baron
SPring-8/RIKEN, Hyogo 679-5148, Japan
(Received 9 January 2008; published 22 May 2008)

The dynamic structure factor $S(Q,\omega)$ of liquid Fe was measured at 1570 °C near the melting point of 1535 °C by using a high-resolution inelastic x-ray scattering (IXS). The IXS spectra obtained show well-defined collective excitations, which is in contrast to predictions based on macroscopic thermodynamics. From the detailed analysis using both a damped harmonic oscillator model and a generalized Langevin formalism, it was found that the value of the specific heat ratio γ and the longitudinal kinematic viscosity ν rapidly decrease with Q. However, even when these Q dependent values are used in the generalized hydrodynamic theory, the width of the inelastic excitations is overestimated by about 1 order of magnitude. A description of the damping of the collective excitation in liquid Fe that agrees with the data is instead obtained by using a modified version of the generalized hydrodynamic theory, in which fast viscoelastic relaxation dominates and thermal dissipation is nearly negligible. Compared to liquid alkali metals, the slow (structural) contribution to the longitudinal viscosity is much larger than the fast viscoelastic contribution for small Q. This might reflect the formation of a stable icosahedral intermediate-range order in liquid Fe.

DOI: 10.1103/PhysRevB.77.174203 PACS number(s): 63.50.−x, 61.20.Ne, 61.25.Mv

I. INTRODUCTION

In recent years, particle dynamics in liquid metals has been intensively investigated due to development of inelastic x-ray scattering (IXS) at third-generation synchrotron radiation sources. The high quality $S(Q,\omega)$ data obtained by using this method have been analyzed by using a damped harmonic oscillator (DHO) model[1] or a generalized Langevin formalism using memory functions.[2] While one would expect the acoustic excitation to disperse with a sound velocity comparable to the thermodynamic one, application of these models shows that this is often not the case, even at a modest (few nm^{-1}) momentum transfer Q. This deviation of the sound velocity from the macroscopic value has been thoroughly discussed in the context of the generalized hydrodynamic theory.[3] However, the damping of the excitation modes, i.e., the width of the inelastic excitation peaks, is not yet well understood.

In a monatomic liquid, the excitation lifetimes are shortened by the heat flow and viscous drag. In the thermodynamic (long-wavelength) limit, the width of the inelastic excitation peaks, WQ^2, can be estimated from macroscopic thermodynamic quantities:[2]

$$W = \frac{1}{2}\left[(\gamma - 1)D_T + \frac{\eta}{\rho}\right]. \quad (1)$$

γ is the ratio of specific heats at constant pressure and constant volume, D_T is the thermal diffusivity, η is the longitudinal viscosity, and ρ is the density. The latter term in the brackets is frequently referred to as the longitudinal kinematic viscosity $\nu\ (=\eta/\rho)$. In general, the thermal term, $(\gamma-1)D_T$, contributes much more than the viscoelastic term, η/ρ, within the thermodynamic limit. Generalized hydrodynamics extends this relation to short wavelengths by allowing the quantities γ and η to be Q dependent. Qualitatively, this is supported, e.g., by the case of liquid Ar, which has a large γ value, $\gamma > 2$, and is well known to have a highly damped sound mode in liquid Ar.[4] Meanwhile, liquid alkali metals have a smaller value for $\gamma \sim 1.1-1.2$ and have less strongly damped sound modes.[5]

Liquid transition metals have γ values intermediate between liquid Ar and liquid alkali metals. For example, liquid Ni has $\gamma \sim 1.88$ near the melting point. In addition, it shows a large shear viscosity value η_s of 5.64 mPa s. Due to this, Bermejo *et al.*[6] carried out an inelastic neutron scattering experiment on liquid Ni, anticipating damped features in inelastic excitation modes. However, they observed well-defined collective excitations in the wide Q range up to about 20 nm^{-1}: regarding the atomic motions on microscopic scales, liquid Ni resembles liquid alkali metals rather than liquid Ar. In response to the experimental result, reasoning from generalized hydrodynamics, they posited a Q dependent $\gamma(Q)$ and $\eta(Q)$, approaching the hydrodynamic value as $Q \to 0$ but strongly decreasing with increasing Q.

Scopigno *et al.*,[5] however, pointed out the inadequacy of the generalized hydrodynamics, i.e., Eq. (1) with the Q dependent $\gamma(Q)$ and $\eta(Q)$, based on two considerations. First,

structural relaxation is frozen in the high-frequency region of interest, while only fast μ relaxation survives. Second, the thermal contribution in Eq. (1) fails already at wave vectors as small as a few nm^{-1} since the adiabatic regime could be replaced by an isothermal one. Consequently, Eq. (1) with the Q dependent $\gamma(Q)$ and $\eta(Q)$ is found to overestimate the linewidth by a factor of 2 in the case of liquid Li.[7]

In this paper, we present IXS spectra of liquid Fe which has a large specific heat ratio, $\gamma=1.72$,[8] and shear viscosity, $\eta_s=5.5$ mPa s. Following Eq. (1), strong damping of the excitation modes would be expected within the context of conventional and generalized hydrodynamics. However, our data show the existence of clear modes with damping about 1 order of magnitude smaller than that expected from generalized hydrodynamics, even allowing for the carefully determined parameters in Eq. (1) depending on Q. This damping is much larger than the factor of 2 seen in liquid Li.[7] Nevertheless, good agreement with our results is obtained by using a modified version of generalized hydrodynamics by Scopigno *et al.*,[5] which is mentioned above. The present result serves to extend this model into the region of large-γ, large-η materials and offers an alternative view of the particle dynamics in liquid metals, which comprises the corresponding microscopic character of the elements.

II. EXPERIMENTAL PROCEDURE

The IXS experiments were performed at the beamline BL35XU of the SPring-8 by using a high energy resolution IXS spectrometer.[9] A monochromatized beam of 4×10^9 photons/s was obtained from a cryogenically cooled Si(111) double crystal followed by a Si (11 11 11) monochromator operating in an extreme backscattering geometry (about 89.98°, 21.75 keV). The same backscattering geometry was used for the energy analysis of the scattered x-ray photons with 12 spherically curved Si analyzers. The energy resolution was determined by the scattering from a Plexiglas sample and values of 1.6–1.9 meV (full width at half-maximum) were found for various analyzer crystals. The Q resolution was set to be about ±0.30 nm^{-1}.

The sample thickness was about 100 μm, being slightly larger than a $1/e$ absorber. The purity of the sample was 99.9999%. It was located in a single-crystal sapphire cell, which was a slight modification of the so-called Tamura-type cell.[10] If the melting temperature of the sample is higher than 1000 °C like Fe, the original type of the sapphire cell can no longer be used for the IXS experiment because the high-temperature ceramics adhesive (SEM-COM Co. Inc., type SCE-1) softens around 1000 °C, and the sample cannot be kept in the sample reservoir. In the present experiment, instead, a reservoirless cell was designed as illustrated in Fig. 1. As seen in the figure, a sample with an appropriate thickness for the x-ray transmission was sandwiched with two closed-end tubes. Then, the tubes were cemented and closed by the high-temperature ceramics adhesive under He gas atmosphere in order to fix the sample thickness even after melting and to avoid chemical corrosion between the sample vapor and the metal heating wire at high temperatures.

The sample and the sapphire cell were placed in a vessel[11] equipped with single-crystal Si windows. The very high temperature of 1570 °C was achieved by using two W resistance heaters and monitored with two W-5%Re/W-26%Re thermocouples. The IXS measurements were carried out between 1.3 and 21.3 nm^{-1} over energy transfers of ±40 or ±50 meV.

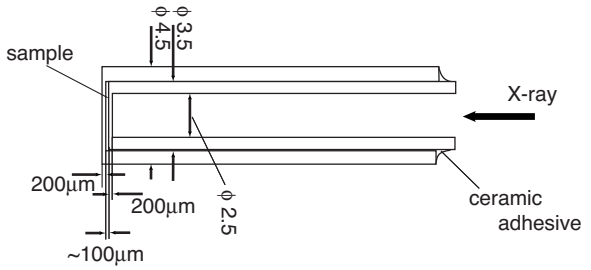

FIG. 1. Cross section of a single-crystal sapphire cell used for the IXS experiment on liquid Fe.

III. RESULTS

Figure 2 shows the selected IXS spectra normalized to the corresponding integral intensity which is identical to $S(Q,\omega)/S(Q)$, except for the resolution broadening. Also given as a dashed line is a typical example of the resolution function. Clear inelastic excitations are seen as peaks or shoulders at both sides of the central line. As mentioned in Sec. I, this result contradicts the hydrodynamic prediction for the excitation damping in this large-γ large-η liquid metal. The energy of the inelastic components shifts with varying Q. This result clearly demonstrates that the inelastic excitations originate from propagating modes, as found earlier in other liquid metals.[5] The width of the quasielastic and inelastic lines becomes broader with increasing Q, and eventually, the inelastic modes look damped. Anomalies indicated by the bars in Fig. 2 result from imperfect corrections of the phonon modes of the sapphire container.

A resolution correction was made by taking a convolution of a model $S(Q,\omega)$ and the experimentally determined resolution function for the measured result. In order to obtain the energy and width of the inelastic excitation modes, we performed an analysis by using a Lorentzian central peak and a DHO excitation,[1] given as

$$\left[\frac{\hbar\omega/k_BT}{1-e^{-\hbar\omega/k_BT}}\right]\frac{A_0}{\pi}\frac{\Gamma_0}{\omega^2+\Gamma_0^2} + \left[\frac{1}{1-e^{-\hbar\omega/k_BT}}\right]\frac{A_Q}{\pi}\frac{4\omega\omega_Q\Gamma_Q}{(\omega^2-\omega_Q^2)^2+4\Gamma_Q^2\omega^2}. \quad (2)$$

Here, A_0 and Γ_0 are the amplitude and the half-width at half-maximum of the central peak, and A_Q, Γ_Q, and ω_Q are the amplitude, width, and energy of the inelastic excitation modes, respectively. The solid curves in Fig. 2 indicate the best fits of the DHO model function convoluted with the resolution function to the experimental data. The DHO model function almost reproduces the experimental data in the whole Q range measured.

The open circles in Fig. 3 indicate the dispersion relation, which is the Q dependence of the ω_Q values, obtained from

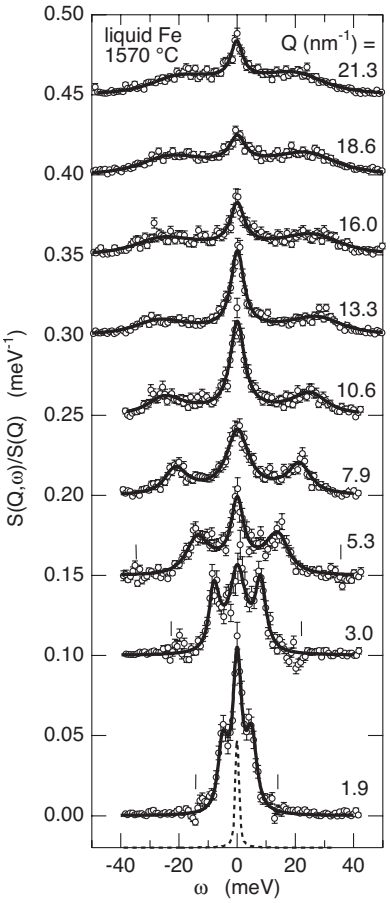

FIG. 2. Selected IXS spectra (circles) normalized to the corresponding integral intensity, which is nearly identical to $S(Q,\omega)/S(Q)$, except for the resolution broadening. The dashed line represents a typical resolution function. The solid curves indicate the best fits of the DHO model function convoluted with the resolution function to the experimental data. The bars represent the energy positions of the phonon modes of the sapphire container.

the fits. The dashed line represents the dispersion of hydrodynamic sound, and its slope is given by the adiabatic velocity of sound (~3800 m/s).[12] As seen in the figure, the dispersion relation of ω_Q in the low Q region locates larger in energy than the hydrodynamic prediction. The increase over the bulk sound velocity is about 11%, which is similar to those in most liquid metals.[5] This so-called positive dispersion can be explained within the framework of the generalized hydrodynamics,[2] where it is shown that frequency-dependent upper and lower limits exist for the propagating speed of longitudinal collective modes. The observed increase toward the upper limit would be related to the onset of a shear viscosity on microscopic scales at high frequencies.

The full triangles in Fig. 3 exhibit the width of the inelastic excitation, Γ_Q. With increasing Q, Γ_Q slowly and almost linearly increases. If the hydrodynamic values of γ, D_T, and η_s are used for Eq. (1), the Γ_Q value is given as the solid curve in Fig. 3, which is much larger than the experimental data, even though the bulk viscosity term is not included. This result indicates that the Q range of the present IXS experiment is, of course, already outside of where the macroscopic hydrodynamic theory can be applied. The modification in the hydrodynamic theory mentioned in Sec. I will be discussed later in detail.

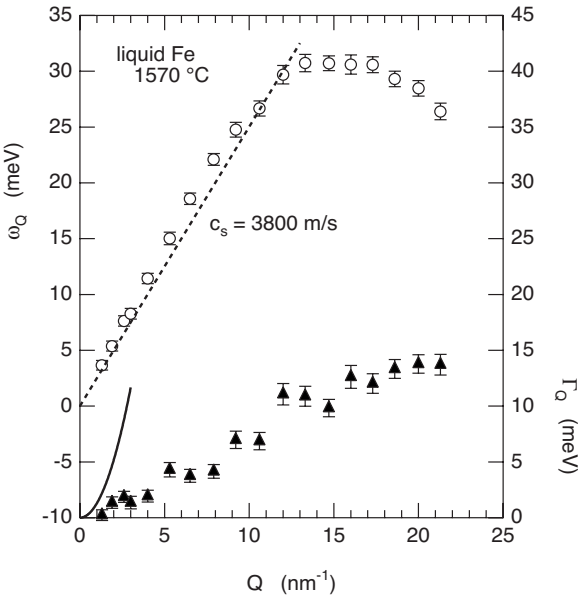

FIG. 3. Dispersion relation (circles) and the width (triangles) of the inelastic excitations in liquid Fe at 1570 °C obtained from the DHO model. The dashed line indicates the dispersion of hydrodynamic sound. The solid curve represents the macroscopic thermodynamic prediction for the widths of the inelastic excitations.

IV. DISCUSSION AND GENERALIZED LANGEVIN ANALYSIS

A practical quantity to present the broadening of the inelastic excitations for liquid systems may be the ratio Γ_Q/ω_Q. The open circles in Fig. 4 show Γ_Q/ω_Q in liquid Fe as a function of reduced momentum transfer Q/Q_p, where Q_p, which is the first maximum position in $S(Q)$, is about

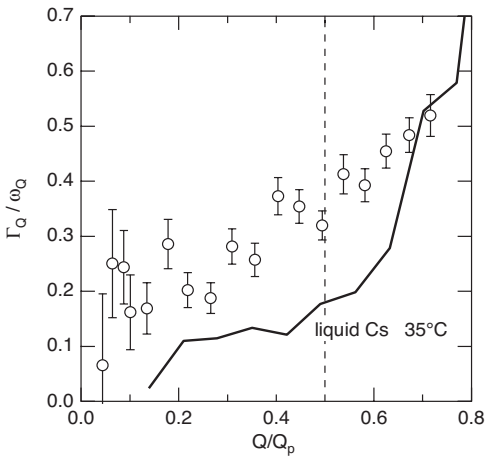

FIG. 4. The ratio Γ_Q/ω_Q of the inelastic excitations in liquid Fe at 1570 °C as a function of reduced momentum transfer Q/Q_p, where Q_p denotes the Q position of the first maximum in $S(Q)$. The solid curve indicates Γ_Q/ω_Q in liquid Cs at 35 °C for the comparison.

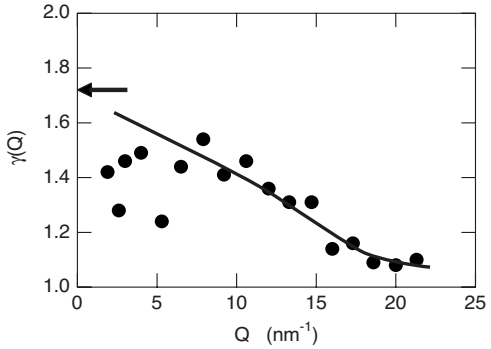

FIG. 5. Q dependence of the heat capacity ratio γ obtained from the Landau–Placzek relation (Ref. 2). The arrow shows the $Q\rightarrow 0$ limit of $\gamma=1.72$. The solid curve is a guide for the eyes.

30 nm^{-1} in liquid Fe. For the comparison, the Γ_Q/ω_Q values in liquid Cs at 35 °C are also exhibited by the solid curve.[13] For liquid Fe, values between 0.07 and 0.37 are found in the first quasi-Brillouin zone, i.e., the Q values up to $Q\sim Q_p/2$ shown as the dashed line. These values are almost twice as large as those in liquid Cs, where the ratio ranges between 0.03 and 0.19 in the corresponding Q zone, indicating almost a half-lifetime of the longitudinal inelastic modes in liquid Fe compared to those in liquid Cs. Although a highly damping feature was expected from the large γ and η_s values in liquid Fe, the actual damping is only slightly larger than that in liquid Cs. The comparison of the damping in liquid Fe with those in liquid alkali metals will be discussed later.

For solving the disagreement on the damping feature in liquid Fe between the present experimental result and the macroscopic hydrodynamic prediction, we shall discuss the Q dependence of the heat capacity ratio $\gamma(Q)$ and longitudinal kinematic viscosity $\nu(Q)$. First, the $\gamma(Q)$ values can be derived by using the Landau-Placzek relation,[2]

$$\frac{I_R(Q)}{2I_B(Q)} = \gamma(Q) - 1, \tag{3}$$

where I_R and I_B are the intensities of the Rayleigh and Brillouin scattering contributions, respectively. These values can be obtained from the energy integrals of the Lorentzian for the quasielastic line and the DHO for the inelastic excitation. Figure 5 shows the γ values obtained as a function of Q. The arrow shows the hydrodynamic value of $\gamma=1.72$, and the solid curve is a guide for the eyes, which will be used for the subsequent analysis. Although the γ data are scattered in the low Q region, it can be observed that $\gamma(Q)$ rapidly decreases with increasing Q and eventually approaches unity beyond $Q=Q_p/2\sim 15$ nm^{-1}. This significant decrease in $\gamma(Q)$ with Q seems to qualitatively contribute to the appearance of the well-defined inelastic excitation modes in liquid Fe.

In order to obtain the Q dependence of the longitudinal kinematic viscosity $\nu(Q)$ from the measured $S(Q,\omega)$ spectra, the second data analysis was carried out by using a generalized Langevin formalism. The basic time correlation probing the collective dynamics in a monatomic fluid (N particles with a mass of m) is the intermediate scattering function,

$$F(Q,t) = \frac{1}{N}\sum_{i,j}\langle - e^{i\mathbf{Q}\cdot\mathbf{r}_i(0)}e^{+i\mathbf{Q}\cdot\mathbf{r}_j(t)}\rangle, \tag{4}$$

where $\mathbf{r}_j(t)$ denotes the position of the jth particle at time t. The initial value $F(Q,t=0)$ corresponds to $S(Q)$. Since $S(Q,\omega)$ is the frequency spectrum of $F(Q,t)$, it is possible to obtain the latter from experimental data with a sufficient quality. Within the generalized Langevin formalism,[14,15] $F(Q,t)$ is determined by

$$\ddot{F}(Q,t) + \omega_0^2(Q)F(Q,t) + \int_0^t M(Q,t-t')\dot{F}(Q,t')dt' = 0, \tag{5}$$

where $M(Q,t)$ is the memory function of the density fluctuations, and $\omega_0^2(Q)=k_BTQ^2/mS(Q)$ is the reduced second frequency moment of $S(Q,\omega)$, giving the lowest limit of the sound velocity at a finite Q as $c_0(Q)=\omega_0(Q)/Q$.

For $M(Q,t)$, we used the well-known approximation containing an exponential decay channel for thermal relaxation and two exponentials for *viscous* relaxation,[16] which is expressed as

$$M(Q,t) = [\gamma(Q)-1]\omega_0^2(Q)e^{-D_TQ^2t} + [\omega_l^2(Q) - \gamma(Q)\omega_0^2(Q)] \times\{[1-A(Q)]e^{-t/\tau_\mu(Q)} + A(Q)e^{-t/\tau_\alpha(Q)}\}. \tag{6}$$

The $\gamma(Q)$ values taken from the Landau-Placzek relation at each finite Q and the $Q\rightarrow 0$ limit of D_T were used for the calculation. In the second term, $\omega_l^2(Q)$ is the reduced fourth moment of $S(Q,\omega)$, which characterizes the instantaneous collective response of the liquid at a finite Q and determines the generalized infinite-frequency velocity (or highest limit of sound velocity in generalized hydrodynamics), $c_\infty=\omega_l(Q)/Q$. τ_μ and τ_α are, respectively, the relaxation rates for the so-called microscopic μ-relaxation process as a faster relaxation dominant over a very short time scale and the α-relaxation (structural relaxation) process as responsible for the long-lasting tail. $A(Q)$ measures the relative weight of the slow viscoelastic decay channel. For simplicity, Eq. (6) is written as[7]

$$\Delta_{th}^2(Q)e^{-D_TQ^2t} + \Delta_\mu^2(Q)e^{-t/\tau_\mu(Q)} + \Delta_\alpha^2(Q)e^{-t/\tau_\alpha(Q)}. \tag{7}$$

The above approach has proven to be useful in describing results of computer simulation studies on simple liquids[16] and also of experimental IXS data on many liquid metals.[5] Details of this model were described in Ref. 7.

For each Q value, the frequency spectrum of $F(Q,t)$ convoluted with the experimentally obtained resolution function was fitted to the present scattering intensity data. The model function fits the data well, which does not seem to be different from the DHO fits shown as the solid curves in Fig. 2. Then, the resolution-deconvoluted line shapes of $S(Q,\omega)$ were built from the fitting parameters, and the corresponding longitudinal current correlation functions, $J(Q,\omega)=(\omega^2/Q^2)S(Q,\omega)$, were calculated from the obtained $S(Q,\omega)$ spectra. The maximum of the $J(Q,\omega)$ function, ω_Q, was used for determining the dispersion relation of the inelastic modes at the finite Q values. The dispersion relation is similar to that obtained from the DHO model analysis shown in Fig. 3,

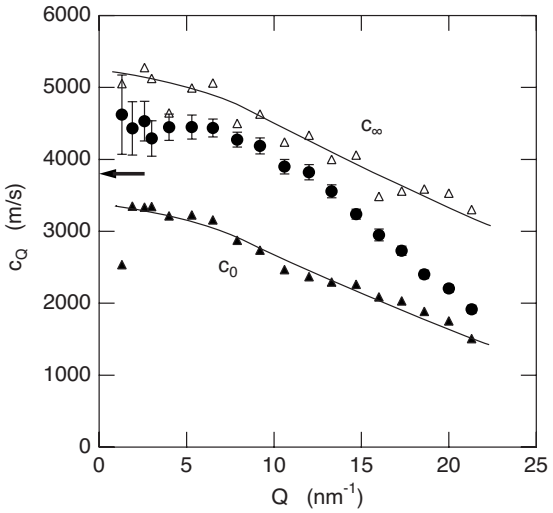

FIG. 6. Dynamical sound velocity c_Q at various Q values obtained from the generalized Langevin analysis (circles). The full triangles indicate the generalized isothermal sound velocity c_0, and the empty triangles the high-frequency values c_∞. The arrow shows the hydrodynamic limit at $Q \to 0$, i.e., the adiabatic sound velocity of 3800 m/s (Ref. 12).

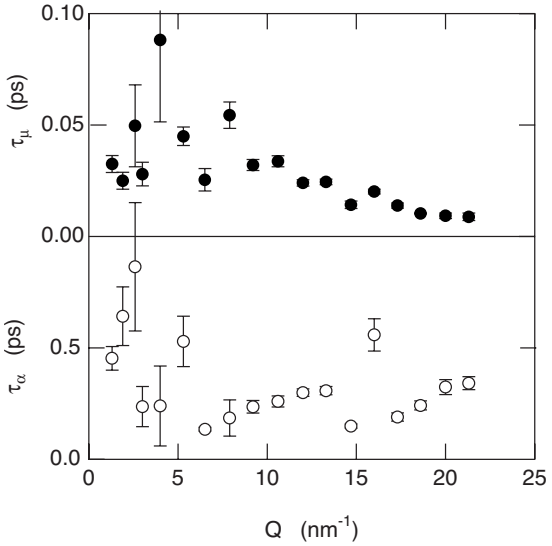

FIG. 7. The viscoelastic relaxation rates, τ_μ (full circles) and τ_α (empty circles), obtained from the present generalized Langevin fits.

and the magnitude of the positive dispersion in the low Q region is 12%, which is slightly larger than that obtained from the DHO model (11%).

The closed circles in Fig. 6 indicate the dynamical sound velocity c_Q $(=\omega_Q/Q)$ at various Q values, ω_Q being obtained from this generalized Langevin analysis. The closed triangles indicate the generalized isothermal sound velocity c_0 $(=\omega_0/Q)$, and the open triangles are the high-frequency values c_∞ $(=\omega_l/Q)$. The arrow shows the hydrodynamic limit at $Q \to 0$, i.e., the adiabatic sound velocity of $\sim$3800 m/s.[12] The c_Q value already deviates from the hydrodynamic value even at the lowest Q values measured, reaches the high-frequency limit c_∞ around $Q=8-10$ nm^{-1}, and again approaches the lower limit c_0 when the Q value reaches the $S(Q)$ maximum. Such a behavior has been commonly observed in several molecular dynamics simulation results of alkali metals[17] and in experimental ones in many liquid metals universally.[5]

Figure 7 shows two viscoelastic relaxation times, τ_μ (full circles) and τ_α (empty circles), obtained by the fits. The slower relaxation time τ_α is almost constant (0.2–0.3 ps), although the data at low Q values are rather scattered. On the other hand, τ_μ seems to gradually decrease with increasing Q.

The Q-dependent (generalized) longitudinal kinematic viscosity $\nu(Q)$ in the generalized Langevin formalism corresponds to the total area of the memory function, which is expressed as

$$\nu(Q) = \frac{\Delta_\mu^2 \tau_\mu + \Delta_\alpha^2 \tau_\alpha}{Q^2}. \tag{8}$$

Figure 8 shows $\nu(Q)$ as a function of Q. As expected, $\nu(Q)$ rapidly decreases with increasing Q. As $\gamma(Q)$ largely decreases with increasing Q, as shown in Fig. 5, this large decrease in $\nu(Q)$ also seems to qualitatively contribute to the appearance of the well-defined inelastic excitation modes in liquid Fe. The dashed arrow indicates the lower limit of the hydrodynamic kinematic longitudinal viscosity at $Q \to 0$, $4\nu_s/3 = 1.04 \times 10^{-6}$ m^2/s, which is experimentally obtained from the hydrodynamic kinematic shear viscosity.[18] By comparing to this hydrodynamic $(Q \to 0)$ value, the $\nu(Q)$ values beyond $Q \sim 3$ nm^{-1} appear reasonable values. Thus, the generalized bulk viscosity would be enhanced in the lower Q region.

By using the above results of the model analyses, we shall quantitatively discuss the damping feature of the collective modes by the generalized hydrodynamic theory. The triangles in Fig. 9 depict the Q dependence of the W values, $W=\Gamma_Q/Q^2$, on a logarithmic scale, Γ_Q being the width of the

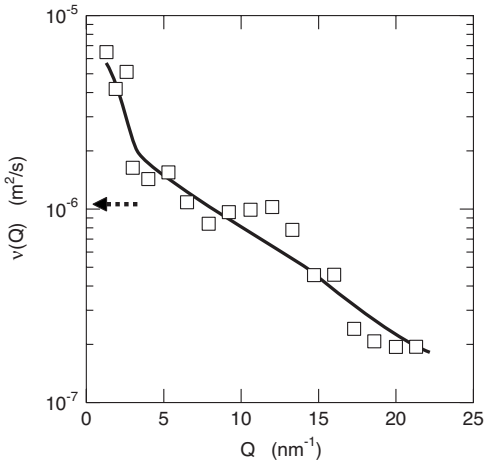

FIG. 8. Logarithmic plot of the Q dependence of the longitudinal kinematic viscosity ν calculated from the generalized Langevin fits. The dashed arrow indicates the lower limit of the hydrodynamic kinematic longitudinal viscosity, $4\nu_s/3 = 1.04 \times 10^{-6}$ m^2/s. The solid curve is a guide for the eyes.

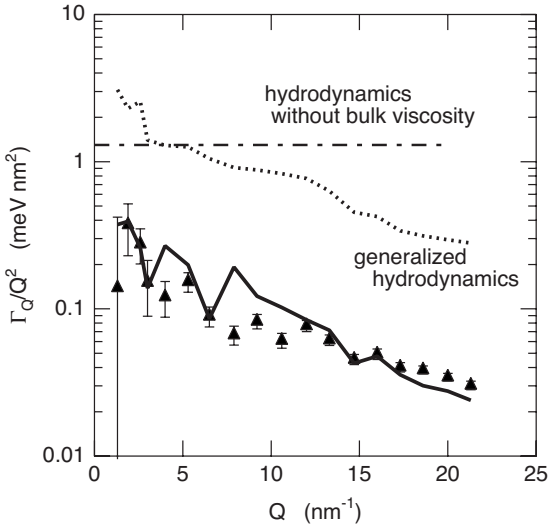

FIG. 9. Logarithmic plot of the Q dependence of the W values, $W=\Gamma_Q/Q^2$. The chain line indicates the macroscopic hydrodynamic prediction given in Eq. (1) by using the $Q\rightarrow 0$ limit of the thermodynamic values. The dotted curve represents the generalized hydrodynamic prediction using the Q-dependent $\gamma(Q)$ and $\nu(Q)$ values. The solid curve shows the W values obtained by the modified version of the generalized hydrodynamic equation, Eq. (9).

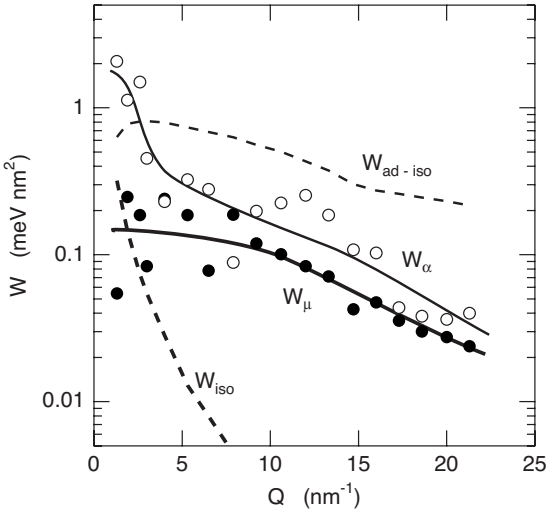

FIG. 10. The full and empty circles indicate, respectively, the fast and slow viscoelastic contributions, W_μ and W_α, to the W values. The solid curves are a guide for the eyes. The thick dashed curve denotes the isothermal term, $W_{\rm iso}$, calculated from the modified version of the generalized hydrodynamic equation, Eq. (9). The thin dashed curve represents the subtracted thermal relaxation term $W_{\rm ad\text{-}iso}$ deduced from the modification of the W equation by Scopigno *et al.* (Ref. 19).

inelastic excitation modes shown as the triangles in Fig. 3. The chain line indicates the macroscopic hydrodynamic prediction calculated from Eq. (1) by using the $Q\rightarrow 0$ limit of the thermodynamic values for γ, D_T, and ν_s. Although the further broadening by the bulk viscosity term is expected, the width of the inelastic excitation modes predicted by the hydrodynamics already gives much larger values than the experimental results, and of course, it cannot reproduce the large Q dependence of W.

The dotted curve in Fig. 9 represents the generalized hydrodynamic prediction by using the Q-dependent $\gamma(Q)$ and $\nu(Q)$ values obtained from the above analyses for Eq. (1). As can be clearly seen in the figure, the predicted values are too large (about 1 order of magnitude) to reproduce the experimentally obtained Γ_Q/Q^2 values although the Q dependence looks similar. Bermejo *et al.*[6] also reported the well-defined inelastic excitations in liquid Ni, which has a very similar thermodynamic nature to liquid Fe. They discussed that "such an apparent paradox was solved some time ago by means of the introduction of a Q-dependent microscopic viscosity $\eta(Q)$ which approaches the hydrodynamic value as $Q\rightarrow 0$ but strongly decreases as Q increases." Such an explanation does not seem to work in the present analysis for liquid Fe. We believe that a quantitative analysis is necessary to discuss the damping of the acoustic modes reported in liquid Ni as well.

Scopigno *et al.*[5,19] discussed the damping of the acoustic modes for liquid Li in the same way and pointed out an overestimate by a factor of about 2 when Eq. (1) was used. Due to the inconsistency between the experimental result and the theoretical prediction, they proposed a modified version of the generalized hydrodynamic equation given as

$$W=\frac{1}{2}\left[(\gamma-1)\frac{c_t^2}{D_T Q^2}+\frac{\Delta_\mu^2\tau_\mu}{Q^2}\right], \tag{9}$$

where c_t is the isothermal velocity of sound, $c_t=c_s/\sqrt{\gamma}$. This formula was based on the idea that in the high-frequency of interest, structural relaxation is frozen (the system is responding as a solid) and, therefore, the viscosity associated to this slow process does not contribute to the sound damping. Moreover, the thermal contribution in Eq. (1) might be incorrect at Q values as large as a few nm^{-1} since the adiabatic regime could be replaced with an isothermal one, as proposed by Scopigno and Ruocco.[19]

The solid curve in Fig. 9 shows the W values obtained by the modified version of the generalized hydrodynamic equation, Eq. (9). As can be clearly seen in the figure, the values reproduce well the experimental results of Γ_Q/Q^2, although both the experimental data and the calculated results are rather scattered due probably to the interference of parameters obtained from the fits, and the Q dependence is slightly different. Thus, the modification of the generalized hydrodynamic theory by Scopigno *et al.*[5,19] leads to the correct estimation for the damping of the acoustic excitation modes.

The solid circles in Fig. 10 show the fast viscoelastic contribution, $W_\mu(=\frac{\Delta_\mu^2\tau_\mu}{2Q^2})$, and the thick dashed curve the isothermal one, $W_{\rm iso}[=\frac{(\gamma-1)c_t^2}{2D_T Q^2}]$ to W, in the modified version of the generalized hydrodynamic equation, Eq. (9). The figure clearly indicates that $W_{\rm iso}$ rapidly decreases with increasing Q and becomes negligible beyond $Q=5$ nm^{-1} compared to W_μ. Thus, it can be concluded that the damping feature of the longitudinal acoustic mode in liquid Fe is dominated by the (fast) viscoelastic relaxation, and the thermal (isothermal) one acts only in the low Q region below 5 nm^{-1}.

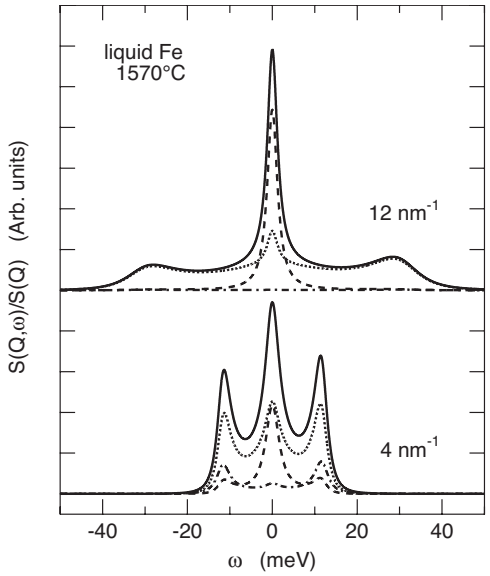

FIG. 11. The resolution-deconvoluted $S(Q,\omega)$ spectra (solid curves) and their fast (dotted curves) and slow (dashed curves) viscoelastic and thermal (chain curves) components at selected Q values of 4 nm^{-1} (lower panel) and 12 nm^{-1} (upper panel).

This conclusion can be confirmed by observing the contributions of the fast relaxation process in $S(Q,\omega)$ spectra. Within the context of the generalized Langevin formalism by using the memory function of Eq. (6), the $S(Q,\omega)$ is expressed as

$$S(Q,\omega) = \frac{S(Q)}{\pi}\,\mathrm{Re}\left\{ i\omega + \omega_0^2(Q) \Big/ \left(i\omega + \frac{\Delta_\mu^2(Q)}{i\omega + 1/\tau_\mu(Q)} + \frac{\Delta_\alpha^2(Q)}{i\omega + 1/\tau_\alpha(Q)} + \frac{\Delta_{th}^2(Q)}{i\omega + D_T Q^2} \right) \right\}^{-1}. \tag{10}$$

From this equation, a linear combination form of $\Delta_\mu^2(Q)$, $\Delta_\alpha^2(Q)$, and $\Delta_{th}^2(Q)$ was obtained in the numerator of the formula, and the contributions of the fast and slow viscoelastic and thermal relaxations were calculated. Figure 11 shows the resolution-deconvoluted $S(Q,\omega)$ spectra (solid curves) at selected Q values of 4 and 12 nm^{-1} and their fast (dotted curves) and slow (dashed curves) viscoelastic and thermal (chain curves) contributions.

At $Q=4$ nm^{-1}, which is shown in the lower panel of Fig. 11, the fast viscoelastic component indicated by the dotted curve dominates the inelastic excitation mode at about 12 meV. On the other hand, the thermal relaxation component given by the chain curve is small compared to the fast viscoelastic relaxation one. The slow viscoelastic relaxation component is negligible in the inelastic excitation modes and mainly contributes to the quasielastic central line. At $Q=12$ nm^{-1}, which is shown in the upper panel of Fig. 11, the above trend becomes much pronounced. The acoustic excitation mode at about 30 meV is totally composed of the fast viscoelastic relaxation process of the memory function, and the thermal and slow viscoelastic relaxation processes do not contribute to it. Thus, it is confirmed that the fast viscoelastic relaxation dominates the damping feature of the longitudinal acoustic mode, and a small portion of the thermal relaxation affects it in the low Q region only.

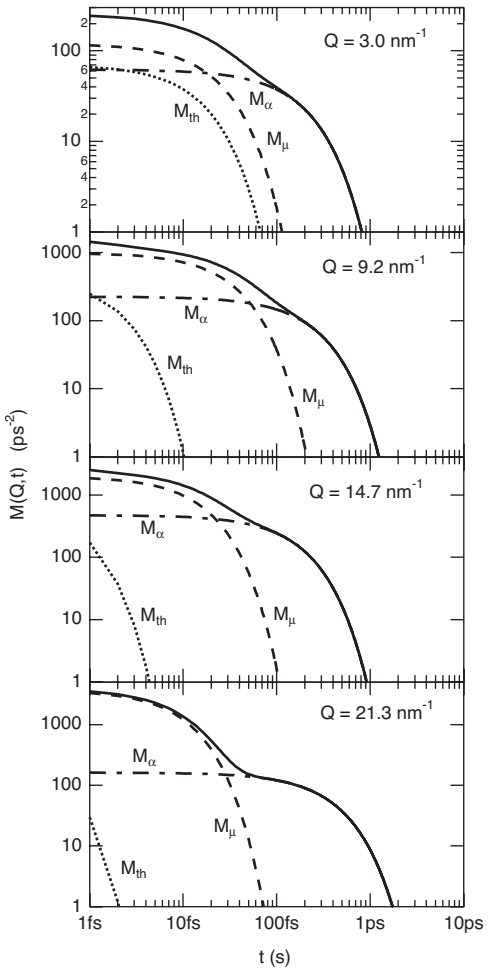

FIG. 12. Selected $M(Q,t)$ functions at several Q values are shown as solid curves. The dotted, dashed, and chain curves indicate parts of the thermal decay channel M_{th}, the fast viscoelastic decay channel M_μ, and the slow viscoelastic decay channel M_α, respectively.

We discuss the time variation in the memory functions obtained from the present generalized Langevin analysis. Figure 12 shows $M(Q,t)$ at selected Q values obtained from the fitting parameters. The $M(Q,t)$ functions can be easily separated into three parts, i.e., the thermal decay channel M_{th} $(=\Delta_{th}^2 e^{-D_T Q^2 t})$, the fast viscoelastic one M_μ $(=\Delta_\mu^2 e^{-t/\tau_\mu})$, and the slow viscoelastic one M_α $(=\Delta_\alpha^2 e^{-t/\tau_\alpha})$, which are drawn by the dotted, dashed, and chain curves, respectively, in Fig. 12.

At the small Q value of 3.0 nm^{-1}, three parts compete in the short time range below ~20 fs, but the largest contribution is M_μ, being about twice as large as the others. With increasing Q, however, the M_{th} contribution decreases more rapidly than M_μ in the short time range, and only the viscoelastic channels dominate $M(Q,t)$ beyond 30–40 fs. In the time range longer than 100 fs, M_μ becomes much smaller than M_α, and the M_α component entirely dominates $M(Q,t)$.

With increasing Q, the decay of M_{th} becomes much faster. On the other hand, the two viscoelastic decay components

gradually change with Q, and they rule over the memory function in the time range beyond 10 fs. The switching from the fast to slow viscoelastic decays happens at the time between several ten femtoseconds and about 100 fs at each Q value measured in the present IXS experiment. In fact, the excitation energies in the present Q range between 3.7 and 30.7 meV correspond to the time range for the density oscillations between about 180 and 20 fs. So, it is reasonable that the memory effect with such a short time regime, i.e., only the fast viscoelastic decay channel can influence the acoustic excitations in the corresponding high-frequency regime.

Unfortunately, the Q dependence of D_T can hardly be obtained due to the small contribution of the thermal decay channel. The D_T value may also gradually decrease with Q as reported for liquid Ne.[20] So, the decay of the thermal channel may become slower than the present calculation, which, however, does not induce any large effect in $M(Q,t)$ in the whole time range. Thus, it is a valid conclusion that the damping of the acoustic excitation mode is closely related to the shorter time domain of the memory function governed by the fast viscoelastic decay channel.

Finally, we compare the results of the present analysis on the damping of the acoustic modes in liquid Fe with those reported for liquid alkali metals, which may help clarify a specific structural character of liquid Fe from the dynamical point of view. As phenomenologically discussed at the beginning of this section using Fig. 4, although a highly damping feature was expected from the large γ and η_s values in liquid Fe, the actual damping is only slightly larger than that in liquid Cs, showing a low damping nature for the excitation modes. Unfortunately, the generalized Langevin formalism was not used for the analysis of the inelastic data of liquid Cs, but the same formula of the memory function with one thermal and two viscoelastic decay channels was applied to other liquid alkali metals also exhibiting well-defined collective excitations in the IXS spectra, such as Li,[7] Na,[21] and K.[22]

The longitudinal kinematic viscosity $\nu(Q)$ was obtained for liquid Li and K. The $\nu(Q)$ value of liquid Li gradually decreases with Q from about 3.5×10^{-6} m^2/s at the smallest $Q=1.4$ nm^{-1} measured, as shown in Fig. 11 of Ref. 7. In the same way, $\nu(Q)$ of liquid K decreases with Q from about 1.8×10^{-6} m^2/s at the smallest $Q=3.2$ nm^{-1} given in Fig. 5 of Ref. 22. The present analysis for liquid Fe provides the $\nu(Q)$ values up to 1.8×10^{-6} m^2/s as shown in Fig. 8, which are very similar to those of liquid Li and K. Thus, the viscoelastic damping of the acoustic modes in liquid Fe can be of magnitude similar to those in liquid alkali metals, as the present experiment revealed.

This is not a surprising result because the viscoelastic damping is not directly governed by the longitudinal viscosity $\eta(Q)$ but by the longitudinal *kinematic* viscosity $\nu(Q)=\eta(Q)/\rho$. Even in the hydrodynamic limit ($Q\rightarrow0$), the kinematic shear viscosity ν_s of liquid Fe is 0.78×10^{-6} m^2/s, while 0.34×10^{-6} m^2/s for liquid Cs calculated from the literature data[18] is almost half of the Fe value. If the damping of the acoustic excitation modes is mostly governed by W_μ as discussed above, and W_μ is proportional to the hydrodynamic ν_s value in any elemental liquid metal, the widths of the inelastic excitations of liquid Fe and Cs given in Fig. 4 are reasonably different from each other.

How does liquid Fe differ from liquid alkali metals in the fast and slow viscoelastic contributions to the $\nu(Q)$? In Fig. 10, the full and empty circles indicate, respectively, the fast and slow viscoelastic contributions, W_μ $(=\frac{\Delta_\mu^2\tau_\mu}{2Q^2})$ and W_α $(=\frac{\Delta_\alpha^2\tau_\alpha}{2Q^2})$, in the W values, which are just half of the corresponding components in $\nu(Q)$. Although the data points are rather scattered due to the parameter interferences in the fitting procedure, W_μ may show a gradual decrease with increasing Q as indicated by the thick solid guide line. On the other hand, an enhancement is seen in the structural viscoelastic contribution W_α at the low Q values below 4 nm^{-1}. At these small Q values, some of the τ_α values exceed the inverse of the resolution width, ~0.42 ps, as seen in the lower panel of Fig. 7. A similar enhancement in τ_α was also reported in liquid Li,[7] Na,[21] and K.[22] However, the product $\Delta_\alpha^2\tau_\alpha$ or the kinematic viscosity $(\Delta_\mu^2\tau_\mu+\Delta_\alpha^2\tau_\alpha)/Q^2$ gradually changes with varying Q, unlike the present Fe result. Thus, we believe that the enhancement in W_α at the low Q values is not artificial. At higher Q values beyond 4 nm^{-1}, W_α decreases in a manner parallel to W_μ with increasing Q as shown by the thin solid guide line, and the ratio W_α/W_μ is approximately 1.5.

Similar information on the ratio W_α/W_μ can be obtained for liquid Li shown in Fig. 10 of Ref. 7. The ratio is about 3 at the lowest Q value of 1.4 nm^{-1} in liquid Li, which is much smaller than the present ratio of about 10 at $Q=1.3$ nm^{-1} in liquid Fe. With increasing Q, the ratio gradually decreases, and in the higher Q range beyond about 3.5 nm^{-1}, it approaches the value of about 1.5, which is similar to that in liquid Fe. The same analysis was also performed for liquid K as given by the inset in Fig. 5 of Ref. 22. In the higher Q range beyond 3 nm^{-1}, the ratio $\Delta_\alpha^2\tau_\alpha/\Delta_\mu^2\tau_\mu$ is mostly less than 2, which is again similar to that in liquid Fe.

It is interesting why the structural viscoelastic component is enhanced in the low Q region in liquid Fe, although this slow viscoelastic decay term does not influence the damping of the acoustic excitations. For discussing the structural viscoelastic decay, it is important to know a specific structural character of liquid Fe by comparing to those of liquid alkali metals. At the beginning stage of the liquid metal science, liquid Fe as well as liquid alkali metals were considered to have a densely packed structure of hard-sphere particles because the $S(Q)$ of these liquid metals can be well described by the Purcus-Yevick approximation for a hard-sphere fluid.[23] However, it is also known that liquid Fe is well supercooled over a wide temperature range, which is an indication of a high activation barrier to form crystal nuclei in the liquid.

Frank[24] postulated that there is a significant amount of an icosahedral intermediate-range order in the well-supercooled melt, which consists of compact arrangements of 13 atoms and possesses a local energy being 8.4% smaller than that of dense-packed fcc or hcp structure of the same number of atoms if atomic interactions are approximated by a Lennard-Jones potential. Recently, the existence of the icosahedral intermediate-range order was experimentally confirmed for the stable (above the melting point) and supercooled liquid Fe by a neutron scattering measurement using a containerless (electromagnetic levitation) technique.[25] On the other hand,

liquid alkali metals are supercooled in a narrow temperature range and no indication of any stable clusters has been reported from both the experimental and theoretical studies on liquid alkali metals.

The formation of such stable clusters should cause a slowing down of the atomic motion or diffusion in liquid Fe because the atoms are trapped into these stable icosahedral clusters in liquid Fe. This slowing down of the atomic motion does not influence the fast viscoelastic decay concerning the cage effect in the melt, but should make the structural viscoelastic decay much slower than that in liquid metals like alkali metals. Thus, it is reasonable to speculate that such an enhancement in the structural viscoelastic decay may originate from the existence of stable icosahedral clusters in liquid Fe, although the size of the icosahedral clusters is slightly larger than the correlation length of the corresponding Q value of about 3 nm^{-1} where the enhancement of W_α starts to occur. Since the existence of the icosahedral clusters was also experimentally observed in liquid Ni and Zr, a similar enhancement in structural viscoelastic decay would be observed in these liquid metals.

For the further analysis of the present $S(Q,\omega)$ data of liquid Fe, the application of a mode coupling theory (MCT) would be an alternative approach. The original version of MCT (Ref. 26) requires detailed knowledge of the interatomic potential. However, a modified version of MCT (Refs. 27 and 28) has recently been applied to the $S(Q,\omega)$ data of molten Ti.[29] Although only the $S(Q)$ and the number density were the inputs to calculate $S(Q,\omega)$ from this version of MCT, the damping of the longitudinal acoustic excitations was reproduced well for molten Ti. However, the MCT calculation produced the dispersion largely deviating from the experimental data and highly depending on the small differences in $S(Q)$ data at small Q values. To our knowledge, the only available $S(Q)$ of liquid Fe was the data measured by Waseda and Suzuki[30] in 1970, which covered the Q range beyond $Q=5$ nm^{-1}. Since precise $S(Q)$ at small Q are necessary even for applying the modified version of MCT to the present data, we shall try to carry out further analyses by using the MCT after measuring the precise $S(Q)$ data, in particular, at small Q values, by a synchrotron radiation experiment.

V. CONCLUSION

The $S(Q,\omega)$ spectra of liquid Fe were measured at 1570 °C near the melting point of 1535 °C by using a high-resolution IXS. The obtained IXS spectra show well-defined collective excitations, in contrast to predictions based on macroscopic thermodynamics. From detailed analysis using both a DHO model and a generalized Langevin formalism, it was found that the values of the specific heat ratio γ and the longitudinal kinematic viscosity ν rapidly decrease with Q. However, even when these Q dependent values are used in the generalized hydrodynamic theory, the width of the inelastic excitations is overestimated by about 1 order of magnitude. Alternatively, a description of the damping of the collective excitation in liquid Fe that agrees with the data is obtained by using a modified version of the generalized hydrodynamic theory in which fast viscoelastic relaxation dominates and thermal dissipation is nearly negligible.[5] Comparing to liquid alkali metals, the slow (structural) relaxation process for the longitudinal viscosity is much larger than that of the fast viscoelastic one in the small Q range in liquid Fe, which may be reflected by a stable icosahedral intermediate-range order formed in this liquid metal.

ACKNOWLEDGMENTS

This work was financially supported by Nippon Sheet Glass Foundation for Materials Science and Engineering. M.I. and K.M. would like to acknowledge a Grant-in-Aid for Scientific Research from the Ministry of Education, Culture, Sports, Science, and Technology, Japan. The IXS experiments were performed at the beamline BL35XU in the SPring-8 with the approval of the Japan Synchrotron Radiation Research Institute (Proposal No. 2005A0567).

*hosokawa@cc.it-hiroshima.ac.jp

[1] B. Fåk and B. Dorner, Institut Laue-Langevin Report No. 92FA008S, 1992 (unpublished).
[2] For example, J. P. Boon and S. Yip, *Molecular Hydrodynamics* (McGraw-Hill, New York, 1980).
[3] For example, U. Balucani and M. Zoppi, *Dynamics of the Liquid State* (Clarendon, Oxford, 1994).
[4] I. M. de Schepper, P. Verkerk, A. A. van Well, and L. A. de Graaf, Phys. Rev. Lett. **50**, 974 (1983).
[5] T. Scopigno, G. Ruocco, and F. Sette, Rev. Mod. Phys. **77**, 881 (2005).
[6] F. J. Bermejo, M. L. Saboungi, D. L. Price, M. Alvarez, B. Roessli, C. Cabrillo, and A. Ivanov, Phys. Rev. Lett. **85**, 106 (2000).
[7] T. Scopigno, U. Balucani, G. Ruocco, and F. Sette, J. Phys.: Condens. Matter **12**, 8009 (2000).
[8] The γ value can be calculated by using the experimental values of heat capacity with constant pressure C_p, temperature T, volume V, thermal expansion coefficient α, and adiabatic compressibility χ_s.
[9] A. Q. R. Baron, Y. Tanaka, S. Goto, K. Takeshita, T. Matsushita, and T. Ishikawa, J. Phys. Chem. Solids **61**, 461 (2000).
[10] K. Tamura, M. Inui, and S. Hosokawa, Rev. Sci. Instrum. **70**, 144 (1999).
[11] S. Hosokawa and W.-C. Pilgrim, Rev. Sci. Instrum. **72**, 1721 (2001).
[12] P. M. Nasch, M. H. Manghnani, and R. A. Secco, J. Geophys. Res. **99**, 4285 (1994).
[13] T. Bodensteiner, Chr. Morkel, W. Gläser, and B. Dorner, Phys. Rev. A **45**, 5709 (1992).
[14] R. Zwanzig, J. Chem. Phys. **39**, 1714 (1963).
[15] H. Mori, Prog. Theor. Phys. **33**, 423 (1965).

[16] D. Lavesque, L. Verlet, and J. Kürkijarvi, Phys. Rev. A **7**, 1690 (1973).
[17] For example, U. Balucani, G. Ruocco, A. Torcini, and R. Vallauri, Phys. Rev. E **47**, 1677 (1993).
[18] T. Iida and R. I. L. Guthrie, *The Physical Properties of Liquid Metals* (Clarendon, Oxford, 1993).
[19] T. Scopigno and G. Ruocco, Phys. Rev. E **70**, 013201 (2004).
[20] H. Bell, H. Moeller-Wenghoffer, A. Kollmar, R. Stockmeyer, T. Springer, and H. Stiller, Phys. Rev. A **11**, 316 (1975).
[21] T. Scopigno, U. Balucani, G. Ruocco, and F. Sette, Phys. Rev. E **65**, 031205 (2002).
[22] A. Monaco, T. Scopigno, P. Benassi, A. Giugni, G. Monaco, M. Nardone, G. Ruocco, and M. Sampoli, J. Chem. Phys. **120**, 8089 (2004).
[23] For example, N. H. March, *Liquid Metals: Concepts and Theory* (Cambridge University Press, Cambridge, 1990).
[24] F. C. Frank, Proc. R. Soc. London, Ser. A **215**, 43 (1952).
[25] T. Schenk, D. Holland-Moritz, V. Simonet, R. Bellissent, and D. M. Herlach, Phys. Rev. Lett. **89**, 075507 (2002).
[26] J. Bosse, W. Götze, and M. Lücke, Phys. Rev. A **17**, 434 (1978).
[27] U. Bengtzelius, W. Götze, and A. Sjölander, J. Phys. C **17**, 5915 (1984).
[28] W. Götze and M. R. Mayr, Phys. Rev. E **61**, 587 (2000).
[29] A. H. Said, H. Sinn, A. Alatas, C. A. Burns, D. L. Price, M. L. Saboungi, and W. Schirmacher, Phys. Rev. B **74**, 172202 (2006).
[30] Y. Waseda and K. Suzuki, Phys. Status Solidi **39**, 669 (1970).